European Journal of Radiology 112 (2019) 186–191

Contents lists available at ScienceDirect

European Journal of Radiology

journal homepage: www.elsevier.com/locate/ejrad

Research article

Whole-tumor histogram analysis of apparent diffusion coefficient in differentiating intracranial solitary fibrous tumor/hemangiopericytoma from angiomatous meningioma

Wenle He[a], Xiang Xiao[a], Xiaodan Li[a], Yihao Guo[b], Liuji Guo[a], Xiaomin Liu[a], Yikai Xu[a], Jun Zhou[c], Yuankui Wu[a,*]

[a] Department of Medical Imaging Center, Nanfang Hospital, Southern Medical University, Guangzhou 510515, China
[b] Faculty of Biomedical Engineering, Guangdong Provincial Key Laboratory of Medical Image Processing, Southern Medical University, Guangzhou 510515, China
[c] Department of Pathology, Nanfang Hospital, Southern Medical University, Guangzhou 510515, China

ARTICLE INFO

Keywords:
Solitary fibrous tumor
Hemangiopericytoma
Angiomatous meningioma
Apparent diffusion coefficient
Histogram analysis

ABSTRACT

Purpose: To assess the role of histogram analysis of apparent diffusion coefficient (ADC) maps based on whole-tumor in differentiating intracranial solitary fibrous tumor/hemangiopericytoma (SFT/HPC) from angiomatous meningioma (AM).

Materials and methods: Pathologically confirmed intracranial SFT/HPC (n = 15) and AM (n = 20) were retrospectively collected and their clinical and conventional MRI features were analyzed. Diffusion-weighted (DW) images (b = 0 and 1000 s/mm^2) were processed with the mono-exponential model. Regions of interest covering the whole tumor were drawn on all slices of the ADC maps to obtain histogram parameters, including mean ADC (ADCmean), median ADC (ADCmedian), maximum ADC (ADCmax), minimum ADC (ADCmin), skewness and kurtosis, as well as the 5th, 10th, 25th, 75th, 90th and 95th percentile ADC (ADC5, ADC10, ADC25, ADC75, ADC90 and ADC95). Differences of histogram parameters between SFT/HPC and AM were compared using *Mann-Whitney U* test. Receiver operating characteristic (ROC) curve was used to determine the diagnostic performance.

Results: The ADCmin (P = 0.001) and ADC5 (P = 0.045) were significantly lower in SFT/HPCs than in AMs, while no significant difference was found in sex, age, conventional MRI features or any other histogram parameters between the two entities (P = 0.051 − 1.000). ADCmin showed the best diagnostic performance (area under curve [AUC], 0.86; sensitivity, 81.3%; specificity, 83.3%) in differentiating SFT/HPC from AM with optimal cutoff value being 569.00 × 10^{-6} mm^2/s, followed by ADC5 (AUC, 0.72; sensitivity, 68.8%; specificity, 75%) with optimal cutoff value being 781.97 × 10^{-6} mm^2/s.

Conclusion: SFT/HPC and AM share similar conventional MR appearances. Whole-tumor histogram analysis of ADC maps may be a useful tool for differential diagnosis, with ADCmin and ADC5 being potential parameters.

1. Introduction

Solitary fibrous tumor/hemangiopericytoma (SFT/HPC) is an uncommon type of neoplasm of meningeal mesenchymal origin [1]. It accounts for about 0.4% of all primary central nervous system tumors with an increasing incidence [2,3]. Radiologically, angiomatous meningioma (AM), a histological subtype of meningioma, is one of the most challenging differential diagnoses for SFT/HPC [4–7]. However, they greatly differ with respect to biological behavior, clinical course, treatment methods and prognosis. SFT/HPC has malignant biological behavior with a high rate of local recurrence and well-known propensity for extracranial metastases, with gross total resection followed by radiotherapy as the main treatment choice [3,8,9]. In contrast, AM is benign and can achieve a good prognosis after surgical resection alone [10–12]. Therefore, accurate preoperative differentiation between SFT/HPC and AM is of vital importance in clinical routine practice.

Conventional MR imaging (MRI) is difficult to reliably distinguish between the two entities [4]. Advanced MRI techniques, such as diffusion weighted imaging (DWI), can provide information on the tissue microstructural characteristics and may be valuable in this regard.

* Corresponding author at: Department of Medical Imaging Center, Nanfang Hospital, Southern Medical University, No.1838 Guangzhou Avenue North, Guangzhou, Guangdong 510515, China.
E-mail address: ripleyor@126.com (Y. Wu).

https://doi.org/10.1016/j.ejrad.2019.01.023
Received 28 October 2018; Received in revised form 16 January 2019; Accepted 21 January 2019
0720-048X/ © 2019 Elsevier B.V. All rights reserved.

Some researchers have studied the role of apparent diffusion coefficient (ADC) measurements in differentiation of these two but with no agreement obtained [4,5,13,14]. This may be mainly due to the research methods they used. They just measured so-called representative areas of the tumor using manual regions of interest (ROIs) for further analysis, which is readily subject to selection bias. Furthermore, they used only one parameter, mean ADC value from regional ROIs, to evaluate the tumors, which fails to reflect the overall spatial heterogeneity of histological features of tumors and thus may dilute or even miss the mild but important differences between them.

Histogram analysis of ADC maps, based on the whole tumor volume, is an objective and robust method that can provide quantitative information on tissue characteristics and tumor heterogeneity [15]. This method has been shown promising in differential diagnosis as well as predicting tumor grade and prognosis [15–19]. Therefore, the purpose of this study was to determine the diagnostic performance of whole-tumor ADC histogram analysis for differentiating SFT/HPC from AM.

2. Materials and methods

2.1. Patients

This study was approved by our institutional review board, and the written informed consent was waived due to the retrospective nature of our study. Twenty-one SFT/HPC and 24 AM cases were searched from January 2014 to October 2018 from the electronic hospital information system and picture archiving and communication system, according to the following including criteria: 1) available pretreatment brain MRI; 2) final diagnosis confirmed by surgery and histopathologic examinations. Six patients with SFT/HPC and 3 patients with AM were excluded because of absence of DWI images. One AM patient only with cystic component was excluded. Finally, 15 patients with SFT/HPC (10 men and 5 women; mean age, 51.1 ± 16.1 years) and 20 patients with AM (12 men and 8 women; mean age, 55.6 ± 8.8 years) were enrolled in the study.

2.2. MRI

All MRI procedures were performed using a 3.0 T GE Signa Excite MRI system (General Electric, Milwaukee, WI, USA) equipped with an eight-channel array head coil. The standard MRI protocol included T1-weighted images (TR/TE, 2500/24 ms, slice thickness, 6 mm, field of view, 240 mm, matrix, 320 × 224); axial T2-weighted imaging (TR/TE, 5100/130 ms, slice thickness, 6 mm, field of view, 240 mm, matrix, 512 × 288). DWI was performed in the axial plane before injection of contrast agent using single-shot diffusion-weighted echo planar imaging. The imaging parameters were as follows: TR/TE, 10000/88 ms, slice thickness, 6 mm, field of view, 240 mm, matrix, 130 × 128, three orthogonal directions with b-value of 0 and 1000s/mm^2. For contrast enhanced T1-weighted image, contrast agent (Gadopentetate dimeglumine injection, Consun, Guangzhou, China) was intravenously bolus injected via a power injector with a flow rate of 2.0–2.5 ml/s at a dose of 0.2 mmol/kg of body weight, followed by a 20 ml bolus of saline with the same injection rate.

2.3. Image analysis

2.3.1. Conventional MRI features analysis

The conventional MRI features, including location (convexity, skull base, falx or parasagittal, posterior fossa), shape (round or oval, lobulated or irregular), T2WI signal relative to the gray matter (hyperintense, isointense, hypointense), enhancement pattern (homogenous enhancement, heterogeneous enhancement), broad-based attachment, dural tail sign, flow void sign (dot-like or tubular structures of low signal intensity due to the blood flow), necrosis or cystic change and bone destruction, were evaluated and compiled by two radiologists (with 15 and 5 years of experience, respectively) in a blind manner. Discrepancies were resolved in consensus during a joint evaluation with a third radiologist (with 20 years of experience).

2.3.2. ADC histogram analysis

ADC maps were calculated automatically using the Func-Tool software program (GE Medical Systems) with a mono-exponential fit of diffusion data from the b-values of 0 and 1000s/mm^2. All MR data were transferred to an independent, personal computer for further analysis. To obtain histograms of ADCs, two independent radiologists (with 10 and 4 years of experience, respectively), who were blinded to the pathological findings, manually placed ROIs covering the whole lesion in each slice on ADC maps using 3D-Slicer (a free open source software platform for biomedical imaging research). Tumor boundaries were determined with reference to the T2-weighted, enhanced T1-weighted, and diffusion-weighted (b-value, 1000s/mm^2) images. Peritumoral vessels and edema and susceptibility artifacts were avoided. The ROIs were slightly smaller in size than visible tumor boundaries to reduce the partial volume effect. A column of ADC values from all voxels of each tumor was extracted. The following parameters were acquired from the ADC histogram: mean ADC (ADCmean), median ADC (ADCmedian), maximum ADC (ADCmax), minimum ADC (ADCmin), skewness, kurtosis and six cumulative histogram parameters including the 5th (ADC5), 10th (ADC10), 25th (ADC25), 75th (ADC75), 90th (ADC90) and 95th (ADC95) percentiles of ADC. Skewness and kurtosis reflect the shape of a histogram and were used to measure the asymmetry of the ADC value distribution around the mean. Skewness is positive if most of the data are concentrated on the left of the histogram and negative if most of the data are concentrated on the right. Kurtosis represented the concentration of values around the mean and reflected the peak of the distribution. In a normal distribution, skewness is 0, and kurtosis is 3 [20]. Measurements of two radiologists were averaged.

2.4. Pathologic examination

All patients underwent gross total resection (GTR). Surgical specimens were routinely fixed in 4% formaldehyde solution, entirely embedded in paraffin blocks, cut at a 4 μm thickness and stained with haematoxylin and eosin (H-E). Immunohistochemical staining using MIB-1 antibody was performed for 15 SFT/HPC and 4 A M to evaluate Ki-67 index. A pathologist (with 15 years of experience) reassessed the pathological results in a blind manner according to the 2016 WHO criteria [1].

2.5. Statistical analysis

All statistical analyses were performed using IBM SPSS Statistics for Windows, Version 23.0 (IBM Corp., Armonk, NY, United States). Inter-reader agreement of conventional MRI features and the measurements of histogram parameters were assessed by using intraclass correlation coefficient (ICC). The ICC value ranging between 0 and 1.00 and was interpreted as follows: 0-0.40, poor agreement; 0.41-0.60, moderate agreement; 0.61-0.80, good agreement; 0.81–1, excellent agreement. Difference of patient age was compared using Student's *t*-test. Differences of sex and conventional MRI features between two groups were compared using Fisher's exact test. Differences of histogram parameters between the SFT/HPC and AM group were compared using the Mann-Whitney *U*-test. Pearson's correlation was performed to evaluate the associations between histogram parameters and Ki-67 index in SFT/HPC. In addition, receiver operating characteristic (ROC) curve was used to evaluate the diagnostic performance of histogram parameters. The area under the ROC curve (AUC), with the 95% confidence interval (CI), as well as cutoff value, sensitivity, and specificity, were computed. Cutoff values were established by calculating the maximal Youden index. All cases were two-sided at a 5% risk.

Table 1
Demographic information and conventional MRI features of SFT/HPC and AM.

Variable	Characteristics	SFT/HPC	AM	*P* value	*ICC*
No. of patients		15	20		
Age (years), Mean ± SD*		51.1 ± 16.1	55.6 ± 8.8	0.339	
Sex	Male	10	12	0.737	
	Female	5	8		
Location	Convexity	3	4	1.000	0.990
	Falx or parasagittal	5	8		
	Skull base	4	5		
	Posterior fossa	3	3		
Shape	Lobulated or irregular	9	11	1.000	0.608
	Round or oval	6	9		
T2WI signal	Hyperintense	5	13	0.183	0.512
	Isointense	7	5		
	Hypointense	3	2		
Enhancement pattern	Homogenous	7	12	0.506	0.623
	Heterogeneous	8	8		
Broad-based attachment	Present	8	14	0.481	0.638
	Absent	7	6		
Dural tail sign	Present	10	15	0.712	0.602
	Absent	5	5		
Flow void sign	Present	11	15	1.000	0.396
	Absent	4	5		
Necrosis or cystic change	Present	6	5	0.467	0.731
	Absent	9	15		
Bone destruction	Present	7	5	0.282	0.634
	Absent	8	15		

Note: Unless otherwise specified, data were tested using Fisher's exact test. * Data were tested using Student's t-test. SFT/HPC, intracranial solitary fibrous tumor/hemangiopericytoma; AM, angiomatous meningioma; ICC, intraclass correlation coefficient; SD, Standard Deviation.

3. Results

No statistical difference was found in age (P = 0.339) or sex (P = 0.687) between SFT/HPC and AM groups (Table 1).

Of the 15 SFT/HPC patients, 3 were classified as WHO grade I, 8 as grade II, and 4 as grade III. Microscopically, dense, spindle and polygonal tumor cells were distributed around microvessels with a staghorn configuration. Mitosis figures were commonly noted, and the Ki-67 proliferation index was averaged to 11.9% ± 11.2. All AM tumors were classified as WHO grade I. Microscopically the tumors were composed of abundance of various vessels on the background of meningothelial elements, with rare mitosis figures noted. Of the 4 AM patients with immunohistochemical staining, Ki-67 index was scored 3% in 1 case, and the remaining 3 cases were all less than 1%.

Conventional MRI features of the two groups are summarized in Table 1. No statistical difference was found ($P = 0.183–1.000$). Poor inter-reader agreement was obtained for the evaluation of signal void of vessel (ICC = 0.396), moderate inter-reader agreement was obtained for T2WI signal (ICC = 0.512), excellent agreements were obtained for tumor location (ICC = 0.990), good agreements were obtained for these remaining features (ICC = 0.602–0.731).

The values of histogram parameters of ADC maps are listed in Table 2. The ADCmin ($P = 0.001$) and ADC5 ($P = 0.045$) were significantly lower in SFT/HPCs than in AMs, while there was no significant difference in ADC10, ADC25, ADC75, ADC90, ADC95, ADCmean, ADCmedian, ADCmax, skewness or kurtosis ($P = 0.051–0.889$). Significant negative correlation was observed between ADCmin and Ki-67 (R = −0.575, P = 0.025), as shown in Fig.1. Excellent inter-reader agreements were obtained for the measurements of histogram parameters, with ICCs of 0.912-0.999. The different percentiles of median ADC value of the two groups are shown in Fig. 2. Representative cases of SFT/HPC and AM are shown in Figs. 3 and 4 show the representative case of each group. The results of ROC analyses are shown in Table 3 and Fig. 5. The AUC in differentiating SFT/HPC from AM was 0.86 (sensitivity, 81.3%; specificity, 83.3%) and 0.72 (sensitivity, 68.8%; specificity, 75.0%) for ADCmin and ADC5, with optimal cutoff value being 569.00×10^{-6} mm^2/s and 781.97×10^{-6} mm^2/s, respectively.

4. Discussion

In daily clinical practice, it is challenging for radiologists to make reliable discrimination between SFT/HPCs and AMs. In this study, we demonstrated that whole-tumor histogram analysis of ADC maps may be of potentially differential usefulness and both ADCmin and ADC5 had a high diagnostic performance.

Conventional MRI is the preferred modality to evaluate intracranial tumors. In the present study, SFT/HPC and AM displayed similarities in the location, morphology, T2WI signal, flow void sign and dural tail sign, which was in good agreement with the report by Meng et al [4]. Some researchers documented that HPC rather than AM was more likely to show cystic or necrosis and heterogeneous enhancement, and to contact the skull bone with a narrow base and cause bone destruction [21,22]. Whereas, our present study did not show significant difference in these signs. This might be related to the subjectivity of these signs which is dependent on individual's experience and thus less reproducible. Of note, WHO grade I of SFT/HPC was excluded in these studies while included in our study (3 grade I cases). The difference in the population might have influenced the results, which might be mild since patients with grade I SFT/HPC accounted for only 20% (3/15) in our study. Also, tumor heterogeneity may lead to the disparity, especially for studies with small sample size.

Whole-tumor histogram analysis of ADC can reliably provide quantitative information on tissue characteristics of the entire tumor and has become an important method for evaluation of brain tumors [18,23]. In the present study, this method demonstrated excellent inter-reader agreement of all ADC index. ADCmin and ADC5 in the SFT/HPC group were significantly lower than those in the AM group, with rather good diagnostic performance. This is mainly because SFT/HPC has a higher regional cellularity than AM, leading to reduction of extracellular space and the restricted diffusion of water molecules, and consequently the reduced ADC value [24–26]. Many studies showed that the minimum ADC value has a significant negative correlation with Ki-67 proliferation index, as shown in the present study, and may reflect the region with the most exuberant tumor cells proliferation [27–29]. Histologically, grade II and III SFT/HPCs (12/15 cases in this

Table 2
Difference of histogram parameters between SFT/HPC and AM group.

	SFT/HPC ($n=15$)	AM ($n=20$)	P value	ICC
ADCmean	992.12(870.87, 1258.74)	1108.23(902.56, 1543.47)	0.378	0.998
ADCmedian	954.75(830.25, 1210.38)	1090.50(902.69, 1553.25)	0.246	0.999
ADCmin	461.00(376.00, 531.00)	768.00(599.75, 865.00)	0.001	0.914
ADCmax	2050.00(1869.00, 2912.00)	1839.00(1412.25, 2540.25)	0.403	0.971
ADC5	729.99(598.00, 936.37)	888.55(730.46, 1253.14)	0.045	0.995
ADC10	761.50(630.88, 984.28)	919.10(771.68, 1308.93)	0.051	0.997
ADC25	832.31(716.38, 1078.31)	988.50(839.16, 1423.84)	0.104	0.999
ADC75	1098.06(934.00, 1469.38)	1173.19(966.19, 1665.56)	0.577	0.998
ADC90	1248.03(1053.93, 1618.38)	1231.50(1019.46, 1782.24)	0.889	0.996
ADC95	1359.58(1180.44, 1713.75)	1273.73(1107.38, 1869.91)	0.745	0.989
Kurtosis	1.96(1.09, 2.68)	0.87(0.00, 3.43)	0.486	0.912
Skewness	1.02(0.54, 1.36)	0.36(-0.04, 1.60)	0.178	0.971

Note: Except for P value and ICC, data are presented as median (interquartile ranges [IQR]). Values are expressed in units of $\times 10^{-6}$ mm^2/s for all ADC histogram parameters except for skewness and kurtosis. SFT/HPC, intracranial solitary fibrous tumor/hemangiopericytoma; AM, angiomatous meningioma; ICC, intraclass correlation coefficient; ADC, apparent diffusion coefficient; ADCn, nth percentile value of cumulative ADC histogram.

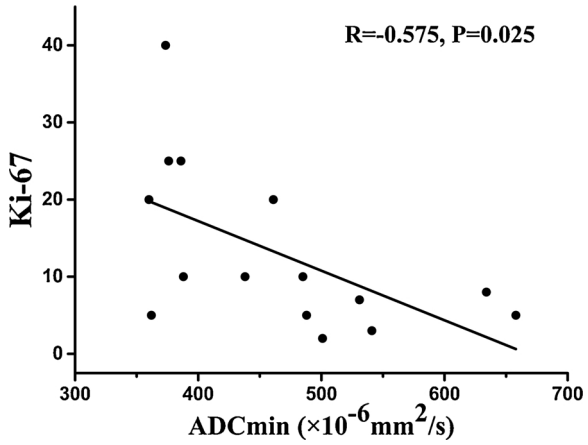

Fig. 1. Scatterplot showing a negative correlation between ADCmin and Ki-67 index of SFT/HPC.

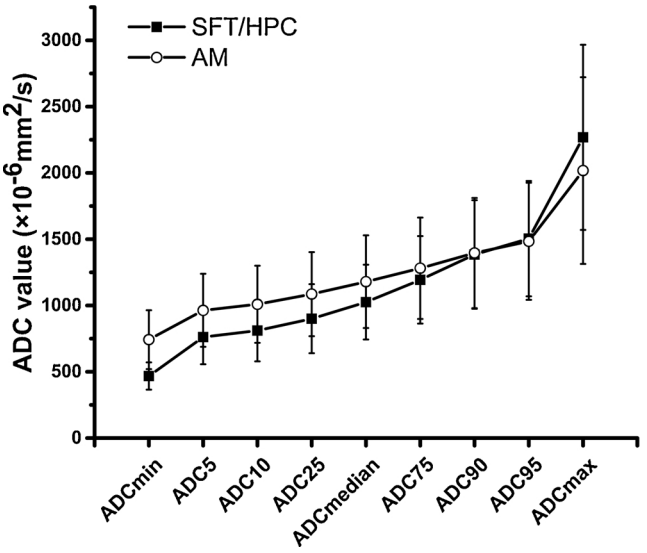

Fig. 2. Line graph demonstrating the median ADC value and their interquartile ranges of two groups at different percentiles. Generally, SFT/HPCs show a lower ADC value than AMs with the differences getting smaller with increasing percentile.

cohort) commonly exhibit high proliferation activity [1,30,31]. In contrast, AMs are mainly composed of vascular components (over 50%) and show low proliferation activity [10]. The mean Ki-67 index (11.9%) in the SFT/HPC group was considerably higher than that of AM in this study. However, Liu et al reported little difference between HPC and AM group in minimum ADC, which was different from our results [32]. This may be because of the different research method used in the present study. Whole-tumor analysis is believed to be able to more reliably obtain the minimum ADC value of the lesion than traditional strategy, which will be helpful to disclose the slight difference between them [18]. Of note, ADC10 showed a trend of being significantly different between the two groups in the present study.

No difference was found in ADCmean and other ADC percentiles between the two groups in this study. This is probably because both types of tumors are hypervascular and have prominent extracellular space surrounding highly vascularized areas, which allows for quick motion of water molecules and thus enables them with high ADC values [33,34]. Moreover, they shared similar necrosis or cystic changes. Meng et al reported the significant difference in ADCmean between them [4], which is contrary to another study by Liu et al [5]. This might imply the relatively limited use of ADCmean derived either from whole-tumor volume analysis or from common methods of manual ROI analysis of solid areas.

Kurtosis and skewness are two important indicators for overall spatial heterogeneity of tumoral characteristics and can provide useful information for the differential diagnosis of tumors [14,35,36]. In this study, however, both groups showed a similar positive skewed distribution (skewness > 0, kurtosis > 0). This may be partly related to the fact that they both are mainly solid tumors with abundant vascular components. Also, the kurtosis and skewness are greatly influenced by the tail configuration of the histogram [37], which was similar between the two groups of tumors owing to significant overlapping of the necrosis or cystic changes.

Our study had several limitations. It was a retrospective study and the sample size was relatively small, so validation in prospective studies with a larger patient cohort is warranted. Also, although the abnormal signal caused by visible DWI artifacts was manually excluded, a few hard-to-find signal abnormalities may still exist and influence the measurement of ADC value. Finally, ADC value in peritumoral edema, which was shown to be able to discriminate HPC from AM in a previous study [5], was not analyzed in our study due to the limitations of our method.

5. Conclusion

In conclusion, our present study showed that conventional MRI features are not sensitive discriminator between SFT/HPC and AM, whole-tumor histogram analysis of ADC maps has the potential to reliably reflect the histopathological differences between them, and ADCmin and ADC5 might be useful parameters in differentiating these

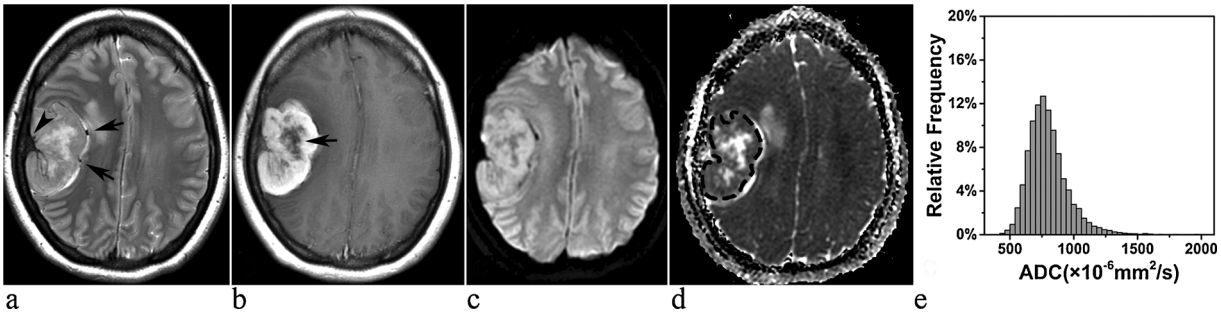

Fig. 3. A 39-year-old woman with SFT/HPC. (a) Axial T2-weighted image shows a large mass in right frontal-temporal convexity, with hyperostosis of the adjacent cranial bone (arrowhead) and peritumoral flow void sign (arrow). (b) Contrast-enhanced T1-weighted image shows avid enhancement and central necrosis (arrow). (c) DWI (b = 1000s/mm^2) shows slightly high signal intensity. (d) Corresponding ADC map with a freehand ROI covering the whole mass (black dashed line). Note that necrosis areas within the tumor were included as well. (e) Histogram of whole lesion shows a relatively lower cumulative ADC value with a flattened peak and ADCmin being 386 × 10^{-6} mm^2/s.

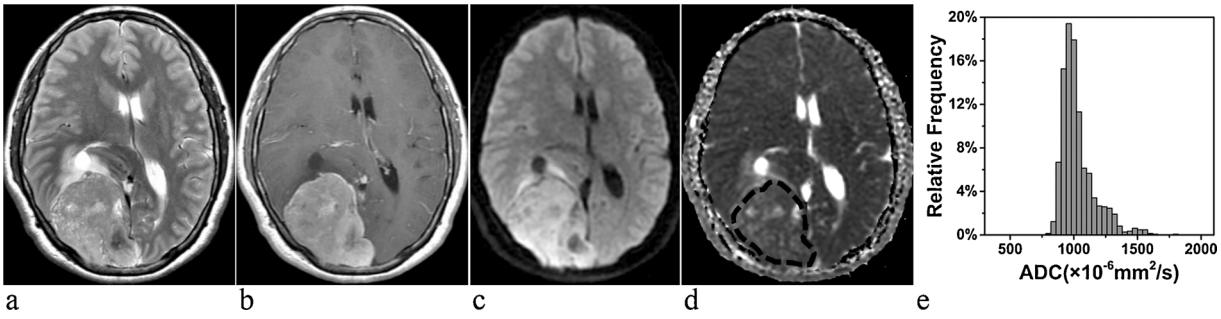

Fig. 4. A 61-year-old woman with AM. (a) Axial T2-weighted image shows a large mass in right occipital convexity. (b) Contrast-enhanced T1-weighted image reveals strong enhancement but no dural tail sign. (c) DWI (b = 1000s/mm^2) shows slightly high signal intensity. (d) Corresponding ADC map delineated with a freehand ROI covering the whole mass (black dashed line). (e) Histogram of the whole lesion shows a relative higher cumulative ADC value with a sharp peak and ADCmin being 807 × 10^{-6} mm^2/s.

Table 3
Diagnostic performance of histogram parameters for differentiating SFT/HPC and AM.

	AUC	Cutoff value (×10^{-6}mm^2/s)	Sensitivity (%)	Specificity (%)	*P* value
ADCmin	0.86(0.72, 1.00)	569.00	81.3	83.3	0.001
ADC5	0.72(0.53, 0.92)	781.97	68.8	75.0	0.046

Note: Data in parentheses are 95% confidence intervals. SFT/HPC, intracranial solitary fibrous tumor/hemangiopericytoma; AM, angiomatous meningioma; AUC, area under the receiver operating characteristic curve; ADC, apparent diffusion coefficient; ADCmin, minimum ADC; ADC5, the 5th percentile value of cumulative ADC histogram. Cutoff values were established by calculating the maximal Youden index.

two entities and thus find clinical applications.

Authors contribution

Wenle He carried out the data collection, analysis and interpretation, and drafted the article. Xiang Xiao, Xiaodan Li, Yihao Guo, Liuji Guo, Xiaomin Liu, Yikai Xu and Jun Zhou participated in the analysis and interpretation of data. All authors read and approved the final manuscript. Yuankui Wu participated in the conception and design of the study, and the analysis and interpretation of data.

Funding

This work was supported by the Science and Technology Program of Guangzhou, China [grant number 201707010003]; and the Special Foundation of President of Nanfang Hospital, Southern Medical University [grant number 2016B026].

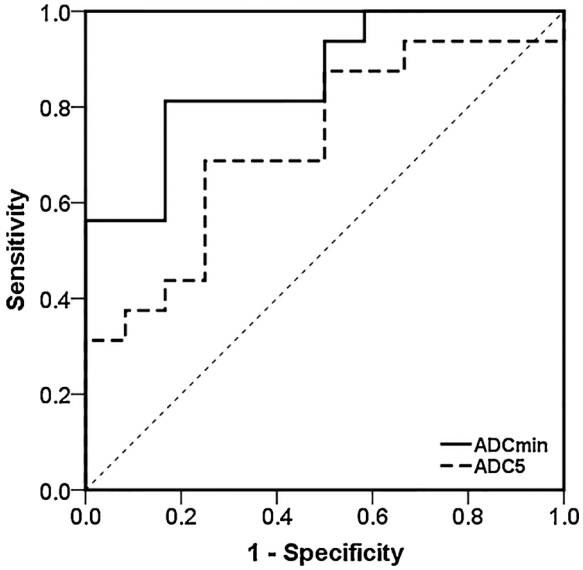

Fig. 5. The ROC curves of ADCmin and ADC5 in differentiation of SFT/HPC and AM. The AUC values of ADCmin and ADC5 were 0.86 and 0.72, respectively.

Role of the funding source

The Funding Source had no role in the writing of the manuscript or the decision to submit it for publication.

Conflict of interest

None.

Declaration of interest

We wish to confirm that there are no known conflicts of interest associated with this publication and there has been no significant financial support for this work that could have influenced its outcome.

References

[1] D.N. Louis, A. Perry, G. Reifenberger, A. von Deimling, D. Figarella-Branger, W.K. Cavenee, H. Ohgaki, O.D. Wiestler, P. Kleihues, D.W. Ellison, The 2016 World Health Organization classification of tumors of the central nervous system: a summary, Acta Neuropathol. 131 (2016) 803–820, https://doi.org/10.1007/s00401-016-1545-1.

[2] T. Ratneswaren, F.R.A. Hogg, M.J. Gallagher, K. Ashkan, Surveillance for metastatic hemangiopericytoma-solitary fibrous tumors-systematic literature review on incidence, predictors and diagnosis of extra-cranial disease, J. Neurooncol. 138 (2018) 447–467, https://doi.org/10.1007/s11060-018-2836-2.

[3] C.J. Kinslow, S.S. Bruce, A.I. Rae, S.A. Sheth, G.M. McKhann, M.B. Sisti, J.N. Bruce, A.M. Sonabend, T.J.C. Wang, Solitary-fibrous tumor/hemangiopericytoma of the central nervous system: a population-based study, J. Neurooncol. 138 (2018) 173–182, https://doi.org/10.1007/s11060-018-2787-7.

[4] Y. Meng, W. Chaohu, L. Yi, P. Jun, Q. Songtao, Preoperative radiologic characters to predict hemangiopericytoma from angiomatous meningioma, Clin. Neurol. Neurosurg. 138 (2015) 78–82, https://doi.org/10.1016/j.clineuro.2015.08.005.

[5] L. Liu, B. Yin, D.Y. Geng, Y. Li, B.Y. Zhang, W.J. Peng, Comparison of ADC values of intracranial hemangiopericytomas and angiomatous and anaplastic meningiomas, J. Neuroradiol. 41 (2014) 188–194, https://doi.org/10.1016/j.neurad.2013.07.002.

[6] N. Zakhari, C. Torres, M. Castillo, T.B. Nguyen, Uncommon cranial meningioma: key imaging features on conventional and advanced imaging, Clin. Neuroradiol. 27 (2017) 135–144, https://doi.org/10.1007/s00062-017-0583-y.

[7] S. Rao, A. Rajkumar, S. Kuruvilla, Angiomatous meningioma: a diagnostic dilemma, Indian J. Pathol. Microbiol. 51 (n.d.) 53–55. http://www.ncbi.nlm.nih.gov/pubmed/18417856 (Accessed 8 October 2018).

[8] S. Kang, S.H. Kim, C. Suh, Solitary fibrous tumor/hemangiopericytoma: treatment results based on the 2016 WHO classification, J. Neurosurg. (2018) 1–8, https://doi.org/10.3171/2017.9.JNS171057.

[9] M.J. Rutkowski, B.J. Jian, O. Bloch, C. Chen, M.E. Sughrue, T. Tihan, I.J. Barani, M.S. Berger, M.W. McDermott, A.T. Parsa, Intracranial hemangiopericytoma: clinical experience and treatment considerations in a modern series of 40 adult patients, Cancer 118 (2012) 1628–1636, https://doi.org/10.1002/cncr.26411.

[10] M. Hasselblatt, K.W. Nolte, W. Paulus, Angiomatous meningioma: a clinicopathologic study of 38 cases, Am. J. Surg. Pathol. 28 (2004) 390–393, https://doi.org/10.1097/00000478-200403000-00013.

[11] Z. Liu, C. Wang, H. Wang, Y. Wang, J.Y. Li, Y. Liu, Clinical characteristics and treatment of angiomatous meningiomas: a report of 27 cases, Int. J. Clin. Exp. Pathol. 6 (2013) 695–702 (Accessed 8 October 2018), http://www.ncbi.nlm.nih.gov/pubmed/23573316.

[12] J. Hwang, D.-S. Kong, H.J. Seol, D.-H. Nam, J.-I. Lee, J.W. Choi, Clinical and radiological characteristics of angiomatous meningiomas, Brain Tumor Res. Treat. 4 (2016) 94–99, https://doi.org/10.14791/btrt.2016.4.2.94.

[13] J.J.S. Shankar, L. Hodgson, N. Sinha, Diffusion weighted imaging may help differentiate intracranial hemangiopericytoma from meningioma, J. Neuroradiol. (2018), https://doi.org/10.1016/j.neurad.2018.11.002.

[14] A.M. El-Ali, V. Agarwal, A. Thomas, R.L. Hamilton, C.G. Filippi, Clinical metric for differentiating intracranial hemangiopericytomas from meningiomas using diffusion weighted MRI, Clin. Imaging 54 (2019) 1–5, https://doi.org/10.1016/j.clinimag.2018.10.018.

[15] F. Davnall, C.S.P. Yip, G. Ljungqvist, M. Selmi, F. Ng, B. Sanghera, B. Ganeshan, K.A. Miles, G.J. Cook, V. Goh, Assessment of tumor heterogeneity: an emerging imaging tool for clinical practice? Insights Imaging 3 (2012) 573–589, https://doi.org/10.1007/s13244-012-0196-6.

[16] N. Just, Improving tumour heterogeneity MRI assessment with histograms, Br. J. Cancer 111 (2014) 2205–2213, https://doi.org/10.1038/bjc.2014.512.

[17] Y. Kang, S.H. Choi, Y.-J. Kim, K.G. Kim, C.-H. Sohn, J.-H. Kim, T.J. Yun, K.-H. Chang, Gliomas: histogram analysis of apparent diffusion coefficient maps with standard- or high- *b* -value diffusion-weighted MR imaging—correlation with tumor grade, Radiology 261 (2011) 882–890, https://doi.org/10.1148/radiol.11110686.

[18] Y.S. Choi, S.S. Ahn, D.W. Kim, J.H. Chang, S. Kang, E.H. Kim, S.H. Kim, T.H. Rim, S. Lee, Incremental prognostic value of ADC histogram analysis over MGMT promoter methylation status in patients with glioblastoma, Radiology 000 (2016) 151913, , https://doi.org/10.1148/radiol.2016151913.

[19] H. Chandarana, A.B. Rosenkrantz, T.C. Mussi, S. Kim, A.A. Ahmad, S.D. Raj, J. McMenamy, J. Melamed, J.S. Babb, B. Kiefer, A.P. Kiraly, Histogram analysis of whole-lesion enhancement in differentiating clear cell from papillary subtype of renal cell cancer, Radiology 265 (2012) 790–798, https://doi.org/10.1148/radiol.12111281.

[20] S. Nougaret, H.A. Vargas, Y. Lakhman, R. Sudre, R.K.G. Do, F. Bibeau, D. Azria, E. Assenat, N. Molinari, M.-A. Pierredon, P. Rouanet, B. Guiu, Intravoxel incoherent motion–derived histogram metrics for assessment of response after combined chemotherapy and radiation therapy in rectal cancer: initial experience and comparison between single-section and volumetric analyses, Radiology 280 (2016) 446–454, https://doi.org/10.1148/radiol.2016150702.

[21] R. Chen, D.C. Peng, Z.L. Hu, H.J. Li, J.K. Zhang, X.Z. Xiao, Differences in MRI findings between intracranial hemangiopericytoma and angiomatous meningioma, Chin. J. Magn. Reson. Imaging 7 (3) (2016) 173–179, https://doi.org/10.12015/issn.1674-8034.2016.03.003.

[22] J.L. Zhou, J.H. Zhao, N. He, C. Dong, Comparison of MRI sign and pathological findings in intracranial hemangiopericytomas and angiomatous type meningioma, J. Chin. Clin. Med. Imaging. 17 (12) (2006) 669–672, https://doi.org/10.3969/j.issn.1008-1062.2006.12.003.

[23] X. Lin, M. Lee, O. Buck, K.M. Woo, Z. Zhang, V. Hatzoglou, A. Omuro, J. Arevalo-Perez, A.A. Thomas, J. Huse, K. Peck, A.I. Holodny, R.J. Young, Diagnostic accuracy of T1-weighted dynamic contrast-enhanced-MRI and DWI-ADC for differentiation of glioblastoma and primary CNS lymphoma, Am. J. Neuroradiol. 38 (2017) 485–491, https://doi.org/10.3174/ajnr.A5023.

[24] R. Murakami, T. Hirai, T. Sugahara, H. Fukuoka, R. Toya, S. Nishimura, M. Kitajima, T. Okuda, H. Nakamura, N. Oya, J. Kuratsu, Y. Yamashita, Grading astrocytic tumors by using apparent diffusion coefficient parameters: superiority of a one- versus two-parameter pilot method, Radiology 251 (2009) 838–845, https://doi.org/10.1148/radiol.2513080899.

[25] S.S. Lu, S.J. Kim, N. Kim, H.S. Kim, C.G. Choi, Y.M. Lim, Histogram analysis of apparent diffusion coefficient maps for differentiating primary CNS lymphomas from tumefactive demyelinating lesions, Am. J. Roentgenol. 204 (2015) 827–834, https://doi.org/10.2214/AJR.14.12677.

[26] T. Sugahara, Y. Korogi, M. Kochi, I. Ikushima, Y. Shigematu, T. Hirai, T. Okuda, L. Liang, Y. Ge, Y. Komohara, Y. Ushio, M. Takahashi, Usefulness of diffusion-weighted MRI with echo-planar technique in the evaluation of cellularity in gliomas, J. Magn. Reson. Imaging 9 (1999) 53–60, https://doi.org/10.1002/(SICI)1522-2586(199901)9:1<53::AID-JMRI7>3.0.CO;2-2.

[27] N. Onishi, S. Kanao, M. Kataoka, M. Iima, R. Sakaguchi, M. Kawai, T.R. Kataoka, Y. Mikami, M. Toi, K. Togashi, Apparent diffusion coefficient as a potential surrogate marker for Ki-67 index in mucinous breast carcinoma, J. Magn. Reson. Imaging 41 (2015) 610–615, https://doi.org/10.1002/jmri.24615.

[28] S. Higano, X. Yun, T. Kumabe, M. Watanabe, S. Mugikura, A. Umetsu, A. Sato, T. Yamada, S. Takahashi, Malignant astrocytic tumors: clinical importance of apparent diffusion coefficient in prediction of grade and prognosis, Radiology 241 (2006) 839–846, https://doi.org/10.1148/radiol.2413051276.

[29] Z. Chen, L. Ma, X. Lou, Z. Zhou, Diagnostic value of minimum apparent diffusion coefficient values in prediction of neuroepithelial tumor grading, J. Magn. Reson. Imaging 31 (2010) 1331–1338, https://doi.org/10.1002/jmri.22175.

[30] C. Bouvier, P. Meſellus, A.M. De Paula, A. Vasiljevic, A. Jouvet, J. Guyotat, K. Mokhtari, P. Varlet, H. Dufour, D. Figarella-Branger, Solitary fibrous tumors and hemangiopericytomas of the meninges: overlapping pathological features and common prognostic factors suggest the same spectrum of tumors, Brain Pathol. 22 (2012) 511–521, https://doi.org/10.1111/j.1750-3639.2011.00552.x.

[31] A.B. Smith, I. Horkanyne-Szakaly, J.W. Schroeder, E.J. Rushing, From the radiologic pathology archives: mass lesions of the dura: beyond meningioma—radiologic-pathologic correlation, RadioGraphics 34 (2014) 295–312, https://doi.org/10.1148/rg.342130075.

[32] G. Liu, Z.Y. Chen, L. Ma, X. Lou, S.J. Li, Y.L. Wang, Intracranial hemangiopericytoma: MR imaging findings and diagnostic usefulness of minimum ADC values, J. Magn. Reson. Imaging 38 (2013) 1146–1151, https://doi.org/10.1002/jmri.24075.

[33] D. She, X. Yang, Z. Xing, D. Cao, Differentiating hemangioblastomas from brain metastases using diffusion-weighted imaging and dynamic susceptibility contrast-enhanced perfusion-weighted mr imaging, Am. J. Neuroradiol. 37 (2016) 1844–1850, https://doi.org/10.3174/ajnr.A4809.

[34] A. Mahajan, V.R.K. Rao, G. Anantaram, A.M. Polnaya, S. Desai, P. Desai, R. Vadapalli, M. Panigrahi, Clinical-radiological-pathological correlation of cavernous sinus hemangioma: incremental value of diffusion-weighted imaging, World J. Radiol. 9 (2017) 330, https://doi.org/10.4329/wjr.v9.i8.330.

[35] H.J. Baek, H.S. Kim, N. Kim, Y.J. Choi, Y.J. Kim, Percent change of perfusion skewness and kurtosis: a potential imaging biomarker for early treatment response in patients with newly diagnosed glioblastomas, Radiology 264 (2012) 834–843, https://doi.org/10.1148/radiol.12112120.

[36] A.D. King, K.-K. Chow, K.-H. Yu, F.K.F. Mo, D.K.W. Yeung, J. Yuan, K.S. Bhatia, A.C. Vlantis, A.T. Ahuja, Head and neck squamous cell carcinoma: diagnostic performance of diffusion-weighted MR imaging for the prediction of treatment response, Radiology 266 (2013) 531–538, https://doi.org/10.1148/radiol.12120167.

[37] P.H. Westfall, Kurtosis as Peakedness, 1905–2014, R.I.P. Am. Stat. 68 (2014) 191–195, https://doi.org/10.1080/00031305.2014.917055.